ACS OMEGA

http://pubs.acs.org/journal/acsodf

Article

# Intensification of $NO_x$ Conversion over Activated Coke by Ozone Oxidation for Sintering Flue Gas at Low Temperatures

Mengze Zhang, Xiao Zhu, Liqiang Zhang,* Yang Li, Jun Li, Xiao Xia, Chunyuan Ma, and Yong Dong*

Cite This: *ACS Omega* 2021, 6, 13484−13495

Read Online

ACCESS | Metrics & More | Article Recommendations

**ABSTRACT:** Denitration (De-$NO_x$) over activated cokes (ACs) for sintering flue gas needs intensification. Gaseous reactions in a gas mixture containing NO, $NO_2$, and $NH_3$, with the effect of $O_2$ concentration and moisture, were taken into consideration in the study of $NO_x$ conversion over ACs. Experimental studies on $NO_x$ conversion with and without $NH_3$ over ACs were conducted using a fixed-bed reactor at 100 °C. The results demonstrated that moisture significantly affected $NO_x$ removal over ACs, especially the $NO_2$ conversion. Under dry conditions, a disproportionation reaction of $NO_2$ over ACs dominated $NO_x$ conversion with no $NH_3$, whereas apparent fast selective catalytic reduction (SCR) over the ACs was observed in the presence of $NH_3$. Regardless of the presence of absence of $NH_3$ in wet mixtures, $NO_2$ adsorption on ACs via the disproportionation route dominated the $NO_x$ conversion. Increasing the $NO_2$/NO ratio in the simulated flue gas enhanced the $NO_x$ conversion rate over ACs. $-C(ONO_2)$ deposition on ACs generated by the disproportionation route inhibited $NO_x$ conversion with time. $O_3$ oxidation was found to be efficient in increasing the $NO_2$/NO ratio and intensifying the $NO_x$ conversion compared with commercially direct $NH_3$-SCR over ACs. Increasing the temperature and decreasing the gas hourly space velocity can promote $NO_x$ conversion over ACs after $O_3$ oxidation. NO oxidized with $O_3$ coupled with $NH_3$ spray and continuous regeneration of ACs is a potential method for removing $NO_x$ from sintering flue gas.

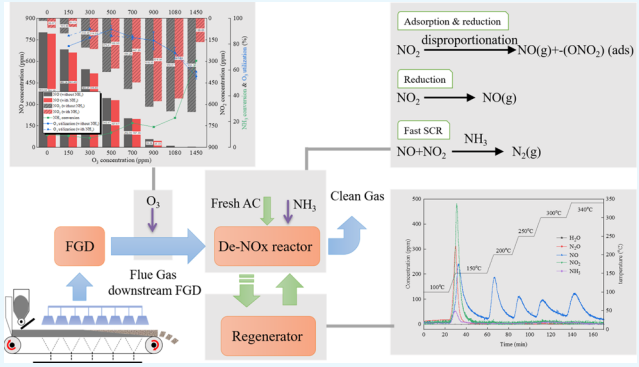


## 1. INTRODUCTION

$SO_2$, $NO_x$, and particulate matter are the dominant flue gas pollutants generated by coal combustion, which remains the leading primary energy supply process in China. After the successful application of pollution control technologies in coal-fired power plants, emissions from other industrial processes have been increasingly attracting attention.[1−5] According to the latest China emission standard published in 2019, the emission limit of particulate matter, $SO_2$, and $NO_x$ for the sintering flue gases is 10, 35, and 50 mg/$Nm^3$, respectively.[6] To meet the emission standard, activated cokes (ACs) have been widely recognized as a potential candidate for $SO_2$ and $NO_x$ removal from sintering flue gases[7] and the schematic diagram of the flue gas purification process using ACs is illustrated in Figure 1.

In this process, $SO_2$ can be captured and converted into sulfuric acid, which can be used in the steel manufacturing. The adsorption of $SO_2$ on ACs as well as the regeneration of ACs have been widely studied and the emission standard of $SO_2$ was achieved.[8−12] $NO_x$ removal by using ACs was carried out after the desulfurization of flue gas, and $NH_3$ has been commonly used as a reductant to react with $NO_x$ to form gaseous nitrogen. ACs act as not only the adsorbent but also a catalyst in the process of $NO_x$ removal. The adsorption properties of NO and $NO_2$ on ACs have been studied in the absence of $NH_3$.[13−17] Some researchers believed that NO was catalytically oxidized to $NO_2$ on the surface of ACs, and $NO_2$

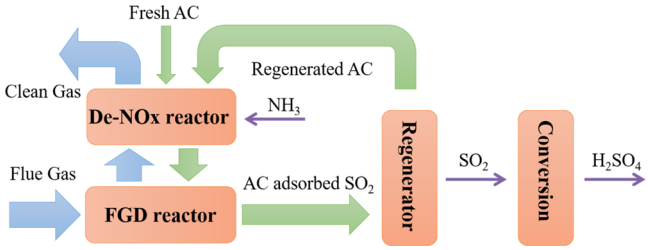


**Figure 1.** Recycling AC sintering flue gas pollutant controlling system.

**Received:** March 30, 2021
**Accepted:** April 29, 2021
**Published:** May 12, 2021

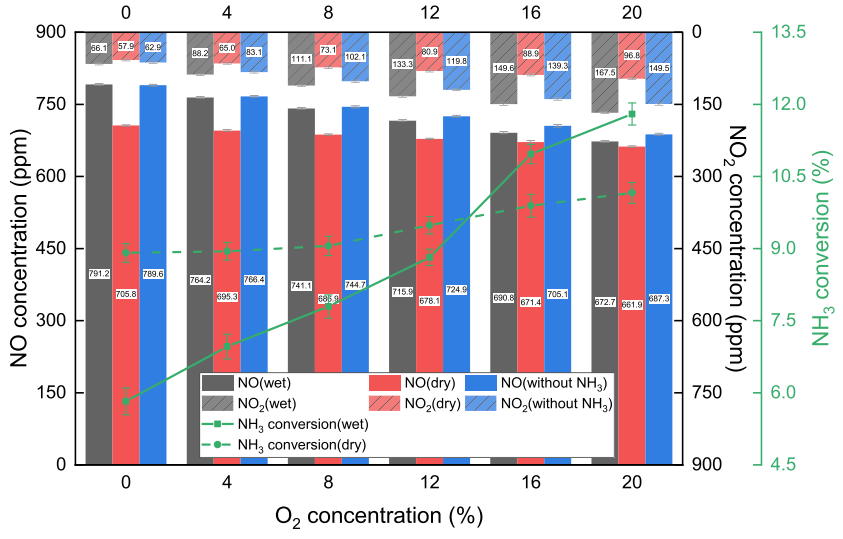


(a)

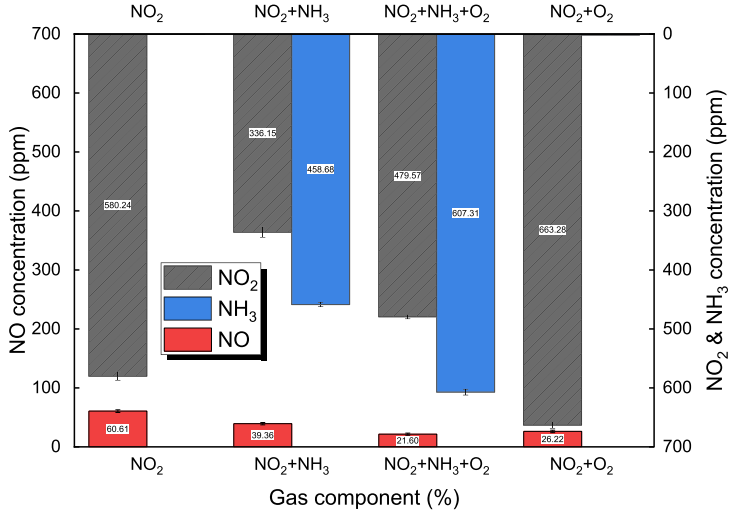


(b)

**Figure 2.** Characteristics of $NO_x$ mixtures with the effect of $O_2$ and $NH_3$ (a) NO mixtures; (b) $NO_2$ mixtures.

was adsorbed and converted into $HNO_3$ in the presence of $O_2$ and moisture.[13,18,19] When $NH_3$ was introduced into this process, ACs acted as a catalyst to convert $NO_x$ into nitrogen via the following selective catalytic reduction (SCR) reaction.[20]

$$NO_x + NH_3 \xrightarrow{\text{catalyst}} N_2 + H_2O$$

Because the temperature for $SO_2$ adsorption at upstream must be controlled below 150 °C, the catalytic activity of ACs is limited for the $NH_3$-SCR reaction.[21−23] Low-temperature $NH_3$-SCR itself has been a research hotspot all over the world.[24] Development of a highly active catalyst at low temperatures in the presence of moisture and $SO_2$ is of interest. Numerous studies have demonstrated that the doping of transition metals such as vanadium,[21,25,26] iron,[22,27,28] manganese,[29] and cerium[30,31] on ACs could effectively improve their catalytic activity at low temperatures. Although the $NO_x$ removal efficiency could reach as high as 40%, the modified ACs still suffered from low-moisture resistance at low temperatures, which limits their application in $NO_x$ removal. Besides, flue gas reheating by using a gas−gas heater fitted downstream of a flue-gas desulfurization (FGD) reactor has also been considered to improve the catalytic activity. In addition to improving the catalytic activity, previous works also demonstrated that the increase of the $NO_2$/NO molar ratio could enhance the $NO_x$ conversion using $NH_3$ as a reductant ($NH_3$-SCR). When the $NO_2$/NO molar ratio = 1, the denitration (De-$NO_x$) rate was found to increase dramatically compared to the $NO_2$/NO molar ratio of 0.[31−33] This fast SCR method consists of the following reaction

$$NO + NO_2 + 2NH_3 \xrightarrow{\text{catalyst}} 2N_2 + 3H_2O$$



https://doi.org/10.1021/acsomega.1c01722
ACS Omega 2021, 6, 13484−13495

To increase the $NO_2$/NO molar ratio, lots of oxidizing regents have been utilized for oxidizing NO to $NO_2$, such as ozone, hydrogen peroxide, chlorine hypochlorite, chlorine dioxide, etc.[34] As the typical oxidizing regent, ozone attracts lots of attention both in investigations and applications.[4,35−38] Among them, NO oxidized by ozone accompanied by a wet scrubber was the most popular technology. NO was oxidized to $NO_2$ or $N_2O_5$, which was more soluble in water than NO, and can be removed using the scrubber. Generally, $N_2O_5$ was preferred when accompanying with a wet scrubber. NO oxidation efficiency reached higher than 90% with $O_3$/NO ⇐ 1 at 100 °C.[35,36] No $N_2O_5$ formed when $O_3$/NO ⇐ 1.[37] Increasing temperature also decreased $N_2O_5$ yield when $O_3$/NO > 1, due to the decomposition of $N_2O_5$ to $NO_2$.[37] $NO_2$ was the mean oxidation product when $O_3$/NO ⇐ 1 at low temperatures. $NO_2$ is more susceptible to be adsorbed than NO. When NO oxidation was accompanied by adsorption, most studies focused on $NO_2$ adsorption to the adsorbent.[13,17]

Studies on the fast SCR method have used $TiO_2$ or AC-supported metal oxide as a catalyst. As for sintering flue gas De-$NO_x$ over ACs, how the fast SCR reaction affects $NO_x$ conversion was rarely studied. Besides, NO adsorption on ACs is always accompanied by oxidation of NO to $NO_2$.[39] Furthermore, sintering flue gas is characterized by high $O_2$ and moisture concentrations. How $NO_x$ adsorption and $NH_3$-SCR reaction affect $NO_x$ conversion on ACs in a sintering flue gas atmosphere was unknown. Ozone ($O_3$) was introduced into gas mixtures for increasing the $NO_2$/NO molar ratio in the experiment to study its effect on $NO_x$ removal.[35] Feasibility of $O_3$ oxidation combined with $NH_3$ spray for $NO_x$ removal over ACs after FGD was also discussed.

## 2. RESULTS

**2.1. Gaseous Characteristics of $NO_x$ and $NH_3$ with the Effect of $O_2$.** Simulated gas flow used in the experiment is a mixture of gases from a cylinder. This would result in difference from the real flue gas. A clear understanding of the gaseous reaction among the gases is fundamental for following studies. Figure 2 illustrates the effect of $O_2$ and $NH_3$ on the composition of a gas mixture containing NO and $NO_2$. Experimental conditions for this study can be found in sets I and II of Table 2. As can be seen from Figure 3a, the $NO_2$ concentration slightly increased with the increase of $O_2$ concentration from 0 to 20%, while the NO concentration decreased continuously. It indicates that part of NO was oxidized to $NO_2$ in the presence of $O_2$. However, no apparent difference in the NO concentration between the gas mixture with and without the addition of $NH_3$ was observed. Compared to wet conditions, both NO and $NO_2$ concentrations in dry gas mixtures were lower. $NO_2$ concentrations increased from 66.1 to 167.5 ppm in a wet gas mixture with the increase of the $O_2$ concentration, while the $NO_2$ concentration increased from 57.9 to 96.8 ppm under dry conditions. $NH_3$ conversion rate increased from 5.8 to 11.8% under wet conditions, which ranged from 8.9 to 10.2% under dry conditions. The conversion of $NH_3$ should include those being oxidized by $NO_x$ or $O_2$, and the oxidized products might include $N_2$ and $NO_x$. According to the analysis of $NH_3$ conversion and NO oxidation in dry and wet mixtures, more $NO_x$ was reduced to $N_2$ by $NH_3$ under dry conditions than that under humid conditions.

Table 1. Chemical Composition and Porous Texture of the Commercial Activated Coke

| elemental analysis (wt %)[a] | C | H | O | N | S |
|---|---|---|---|---|---|
| | 83.76 | 1.32 | 0.89 | 0.76 | 0.3 |
| porous texture | $S_{BET}$ ($m^2$/g) | $V_{total}$ ($cm^3$/g) | $V_{mic}$ ($cm^3$/g) | $V_{meso-macro}$ ($cm^3$/g) | $D$ (nm) |
| | 192.26 | 0.109 | 0.054 | 0.055 | 2.28 |

[a]Air-dry; $S_{BET}$: specific surface area; $V_{total}$: total pore volume; $V_{mic}$: micropore volume; $V_{meso-macro}$: mesopore and macropore volume; and $D$: average pore size.

Figure 3b illustrates the change in composition of wet $NO_2$ balanced with $N_2$ by the addition of $O_2$ and/or $NH_3$. It can be found that NO was detected in all experiments, indicating that $NO_2$ was decomposed into NO and $O_2$ at an experimental temperature of 100 °C. Compared with pure $NO_2$ balanced with $N_2$, $O_2$ could inhibit the $NO_2$ decomposition as the NO concentration decreased from 60.61 to 26.22 ppm by adding 20% $O_2$ into the gas mixture. It can be seen from Figure 3b that the addition of $NH_3$ can effectively convert $NO_2$ into $N_2$. Only 336.15 ppm $NO_2$ and 39.36 ppm NO were detected at the outlet of the reactor, which means over 50% of the $NO_2$ was converted. However, the conversion decreased to less than 32% in the presence of 20% $O_2$, being indicative of the inhibition effect of $O_2$ or the oxidized atmosphere on the gaseous reaction between $NH_3$ and $NO_2$.

**2.2. $NO_x$ Conversion over ACs under Dry and Humid Conditions.** Water vapor is believed to have a significant impact on $NO_x$ conversion over ACs. Sintering flue gas features high moisture. $NO_x$ conversion over the commercial ACs under dry and humid conditions was conducted, and the results are shown in Figure 4. Comparable NO and $NO_2$ concentrations were compounded in the humid or dry mixtures (set III from Table 2). With increasing experimental time, the $NO_2$ concentration at the outlet of the reactor decreased and leveled off at about 35 ppm under both humid and dry conditions. NO concentration from downstream of a fixed-bed reactor was 51 ppm lower than the NO concentration at the inlet under dry conditions, while 37 ppm higher than the inlet NO concentration in the presence of moisture. The drop of NO and $NO_2$ concentrations in the dry mixture is derived from the fast SCR reaction and $NO_2$ adsorption.

According to the results reported in the literature,[15−17,40] there are two main routes for $NO_2$ adsorption on ACs:

(i) $NO_2$ was adsorbed on −C(O) or −C(*) complexes as $-C(ONO_2)$ or $-C(NO_2)$.

$$-C(*) + NO_2 \rightarrow -C(NO_2)$$

$$-C(O) + NO_2 \rightarrow -C(ONO_2)$$

This can be defined as the nondisproportionation route.

(ii) A pair of adsorbed $NO_2$ ($-C(NO_2)$) on one active site or two adjacent active sites reacts through the disproportionation route

$$2 \times NO_2 \rightarrow -C(ONO_2) + NO$$

When $NO_2$ was adsorbed through the disproportionation route, the adsorption of 2 M $NO_2$ will release 1 M NO and leave 1 mol of $-C(ONO_2)$ on the AC surface. Operation conditions, such as temperature, $O_2$ concentration, and


https://doi.org/10.1021/acsomega.1c01722
ACS Omega 2021, 6, 13484−13495

**Table 2. Experimental Conditions**

| sets | carrier gas (500 mL/min) | descriptions |
|---|---|---|
| set I | i: N2 + (0, 4, 8, 12, 16, 20%) $O_2$ + 900 ppm NO + 900 ppm $NH_3$; ii: N2 + (0, 4, 8, 12, 16, 20%) $O_2$ + 8% $H_2O$ + 900 ppm NO + 900 ppm $NH_3$; iii: N2 + (0, 4, 8, 12, 16, 20%) $O_2$ + 8% $H_2O$ + 900 ppm NO | gaseous reaction at 100 °C |
| set II | i: $N_2$ + 8% $H_2O$ + 700 ppm $NO_2$; $N_2$+ 8% $H_2O$ + 700 ppm $NO_2$ + 700 ppm $NH_3$; ii: N2 + 20% $O_2$ + 8% $H_2O$ + 700 ppm $NO_2$ + 700 ppm $NH_3$; iii: N2 + 20% $O_2$ + 8% $H_2O$ + 700 ppm $NO_2$ | gaseous reaction at 100 °C |
| set III | i: N2 + 20% $O_2$ + 8% $H_2O$ + 900 ppm NO + 900 ppm (if present) $NH_3$ ii: N2 + 20% $O_2$ + 750 ppm NO + 150 ppm $NO_2$ + 900 ppm (if present) $NH_3$ | $NO_x$ conversion over 1 g ACs at 100 °C |
| set IV | i: N2 + 20% $O_2$ + 450 ppm NO + 450 ppm $NO_2$ + 900 ppm $NH_3$ ii: N2 + 20% $O_2$ + 700 ppm $NO_2$ + 900 ppm $NH_3$ | $NO_x$ conversion over 1 g ACs at 100 °C |
| set V | i: $N_2$ | regeneration of ACs (set IV-i) |
| set VI | i: N2 + 20% $O_2$ + 8% $H_2O$ + 900 ppm NO + (0, 150, 300, 500, 700, 900, 1080, 1450 ppm) $O_3$ ii: N2 + 20% $O_2$ + 8% $H_2O$ + 900 ppm NO + 900 ppm $NH_3$ + (0, 150, 300, 500, 700, 900, 1080, 1450 ppm) $O_3$ | gaseous reaction at 100 °C |
| set VII | i: N2 + 20% $O_2$ + 8% $H_2O$ + 900 ppm NO + 900 ppm $NH_3$ + 500 ppm $O_3$ | $NO_x$ conversion over ACs at 100, 180, 250 °C |
| set VIII | i: N2 + 20% $O_2$ +8% $H_2O$ + 900 ppm NO + (0, 900, 1800 ppm) $NH_3$ + 500 ppm $O_3$ | $NO_x$ conversion over 4 g ACs at 100 °C |

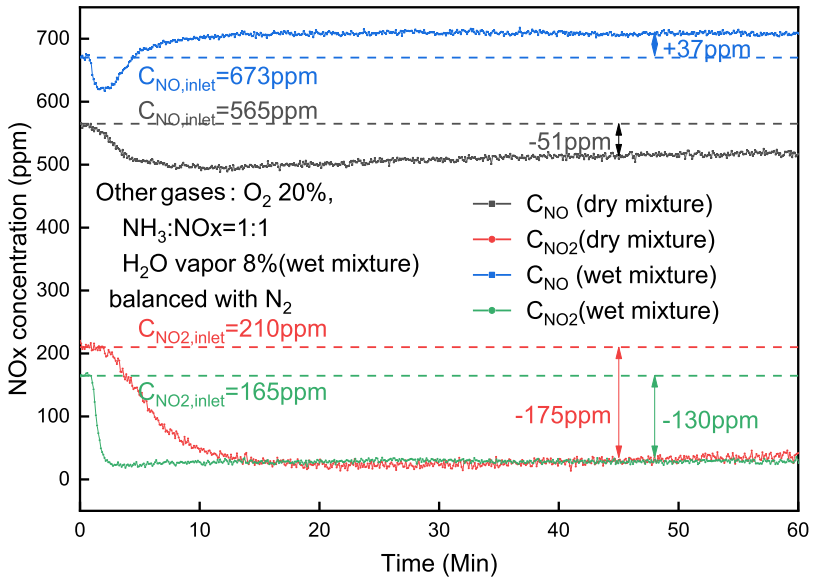


**Figure 3.** $NO_x$ concentrations after ACs under dry and humid conditions.

moisture, play an important role in determining the fraction of $NO_x$ conversion via nondisproportionation and disproportionation routes. The increase of the NO concentration and the drop in the $NO_2$ concentration under wet conditions implied that $NO_2$ adsorption over ACs was dominated by the disproportionation route in the presence of $H_2O$.

$NO_x$ conversion over ACs with $NH_3$ supposed to be derived from the complex interaction between $NO_2$ adsorption through the two routes and the $NH_3$-SCR reaction. Transient reaction analyses were conducted under wet and dry conditions, respectively, to investigate the effect of those processes on $NO_x$ conversion.

Figure 5 shows the change in concentrations of NO and $NO_2$ along with the reaction time under dry conditions. When experiment was conducted without the addition of $NH_3$, the $NO_2$ concentration sharply dropped to nearly zero at the initial state and then slowly increased to the initial $NO_2$ concentration in 294 min. A reverse trend was observed for the NO concentration, which rapidly increased to about 624 ppm that was higher than the initial NO concentration and then slowly dropped to the level equal to the initial concentration. In comparison, the decrease in the concentration of $NO_2$ is about twice the increase in the concentration of NO, indicating that the increase of the NO concentration is mainly attributable to the $NO_2$ adsorption on ACs via the disproportionation route. When $NH_3$ was introduced to the mixture at 294 min, the NO concentration sharply dropped within 20 min and remained stable at about 36 ppm, which was much lower than the initial NO concentration. Meanwhile, the $NO_2$ concentration rapidly dropped to near zero and then slowly increased, which was still much lower than the initial $NO_2$ concentration after 356 min. It can be found from Figure 5 that the $NO_2$ conversion in the presence of $NH_3$ could be divided into two parts: the reduction of $NO_2$ and NO to $N_2$ via fast $NH_3$-SCR (blue area) and the adsorption of $NO_2$ through a nondisproportionation route (gray area). There was no significant increase of the NO concentration being found when $NH_3$ was introduced, which meant that the adsorption of $NO_2$ on ACs via a disproportionation route was limited in the presence of $NH_3$. However, as aforementioned, without the


https://doi.org/10.1021/acsomega.1c01722
ACS Omega 2021, 6, 13484−13495

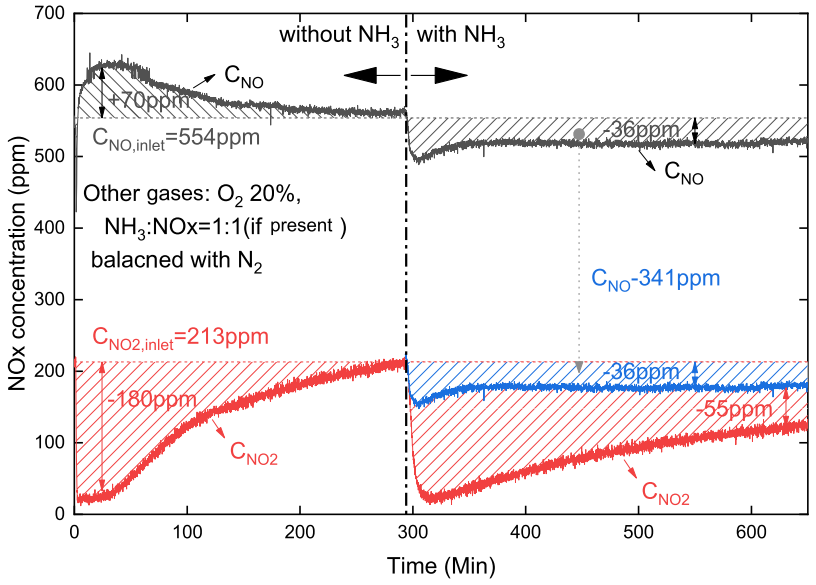


**Figure 4.** $NO_x$ transient conversion over ACs with the effect of $NH_3$ in dry mixtures.

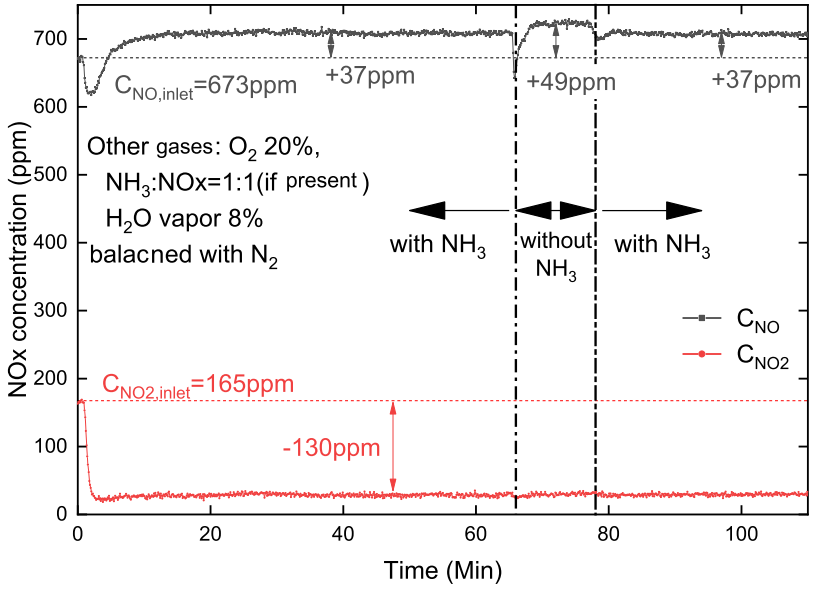


**Figure 5.** $NO_x$ transient conversion over ACs with the effect of $NH_3$ under wet conditions.

addition of $NH_3$, $NO_2$ adsorption on ACs via a disproportionation route played the dominant role in $NO_2$ removal.

Figure 6 shows the effect of $NH_3$ on $NO_x$ conversion over ACs under wet conditions. When $NH_3$ flow was turned off, no significant change in the $NO_2$ concentration was observed, whereas the NO concentration slightly increased. When $NH_3$ flow was turned on again, the NO concentration decreased by 12 ppm, while it was still higher than the initial NO concentration, which means that the addition of $NH_3$ partially inhibited the $NO_2$ conversion via a disproportionation route under wet conditions. However, the $NO_2$ concentration remained unchanged, indicating that the addition of $NH_3$ had no contribution to $NO_2$ removal under wet conditions. Hence, it can be concluded that increasing the $NO_2$/NO ratio supposed to enhance the $NO_x$ conversion ratio.

Figure 7 illustrates the $NO_x$ conversion rate along with reaction time with different $NO_2$/NO ratios. $NO_x$ conversion was only about 12% and remained stable during the experiment period when the $NO_2$/NO ratio was 0.25. When the $NO_2$/NO ratio increased to 1.21, the $NO_x$ conversion rate was about 30% at the initial stage and decreased linearly to about 3% after 300 min. With a further increase of the $NO_2$/NO ratio to 24, the $NO_x$ conversion ratio reached 46% at the initial stage and then linearly decreased to about 20% and maintained at about 20% after 250 min. The above results confirmed that increasing the $NO_2$/NO ratio could effectively improve the $NO_x$ conversion rate, while further investigation is required to explain why the $NO_x$ conversion rate decreased along with reaction time at a $NO_2$/NO ratio higher than 0.25.

Figure 8 shows the breakthrough curves of $NO_2$ conversion over ACs at a $NO_2$/NO ratio of 1.21 and 24 under wet conditions. A significant decrease of the $NO_2$ concentration and an increase of the NO concentration compared with initial concentration were observed, indicating that the disproportionation route of $NO_2$ adsorption is dominant in $NO_x$ conversion at $NO_2$/NO = 24 and 1.21. Different from the


https://doi.org/10.1021/acsomega.1c01722
ACS Omega 2021, 6, 13484−13495

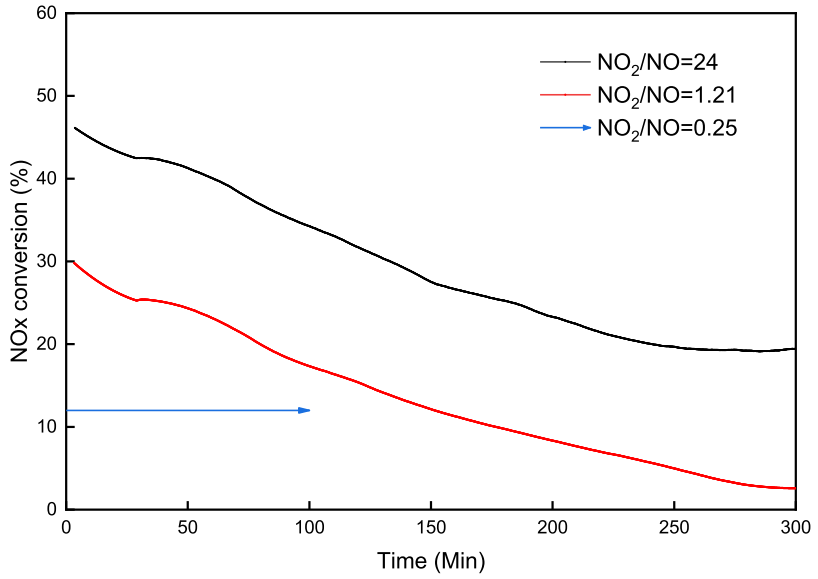


**Figure 6.** $NO_x$ conversion over ACs with the effect of the $NO_2/NO$ ratio.

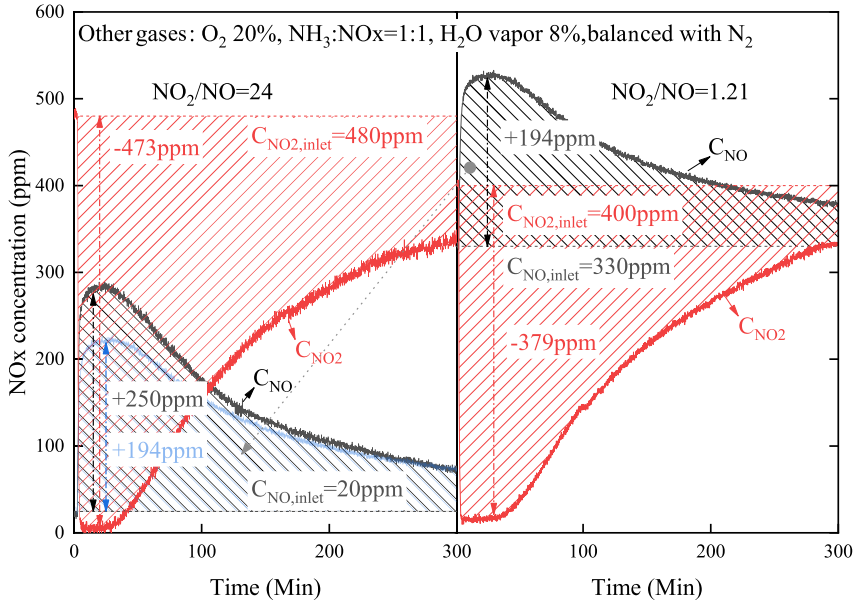


**Figure 7.** Breakthrough of $NO_2$ over ACs in wet mixtures.

stable NO and $NO_2$ outletconcentrations in the ratio $NO_2/NO$ = 0.25, the $NO_2$ concentration increased slightly after reaching nearly zero and the NO concentration decreased slightly after cresting. The adsorbed $NO_2$ in the form of $-C(ONO_2)$ occupied the active sites on the AC surface. The active sites were reduced with the increase of the adsorbed $NO_2$ molecules, which resulted in the breakthrough of $NO_2$. The initial $NO_2$ concentration of the gas mixture with a $NO_2/NO$ ratio of 0.25 is too low, and the adsorption time was not long enough to achieve the breakthrough of $NO_2$.

Figure 9 shows the reduction percentage of $NO_2$, calculated based on the production of NO (gray shadow in Figure 8), and the adsorption percentage of $NO_2$, calculated by subtracting the reduced $NO_2$ from the total $NO_2$ conversion (red shadow in Figure 8), along with reaction time, within the first 150 min, the $NO_2$ reduction rate was almost equal to the $NO_2$ adsorption rate. This was consistent with the disproportionation route. After 150 min, $NO_2$ reduction was getting higher than $NO_2$ adsorption and the difference increased along with reaction time. The decrease of $NO_2$ reduction and adsorption was due to the reducing active sites on ACs for the formation of $-C(ONO_2)$ along with reaction time. The production of NO did not follow the production of $-C(ONO_2)$. This means that the direct reduction of $NO_2$ to NO occurs, which might not make any contribution to final $NO_x$ conversion.

According to Gao[15] and Jeguirim,[40] the adsorbed $NO_2$ would release NO and leave $-C(O)$ on the surface of ACs. Generally, $-C(O)$ would further react with $NO_2$ to form $-C(ONO_2)$, which follows the disproportionation route. With the increase of the adsorption time, not every $-C(O)$ would react with $NO_2$, which resulted in a higher $NO_2$ reduction rate than the adsorption rate as shown in Figure 9.

### 2.3. $NO_x$ Conversion over ACs with Ozone Oxidation.

As discussed above, a higher $NO_2/NO$ ratio could improve the


https://doi.org/10.1021/acsomega.1c01722
ACS Omega 2021, 6, 13484−13495

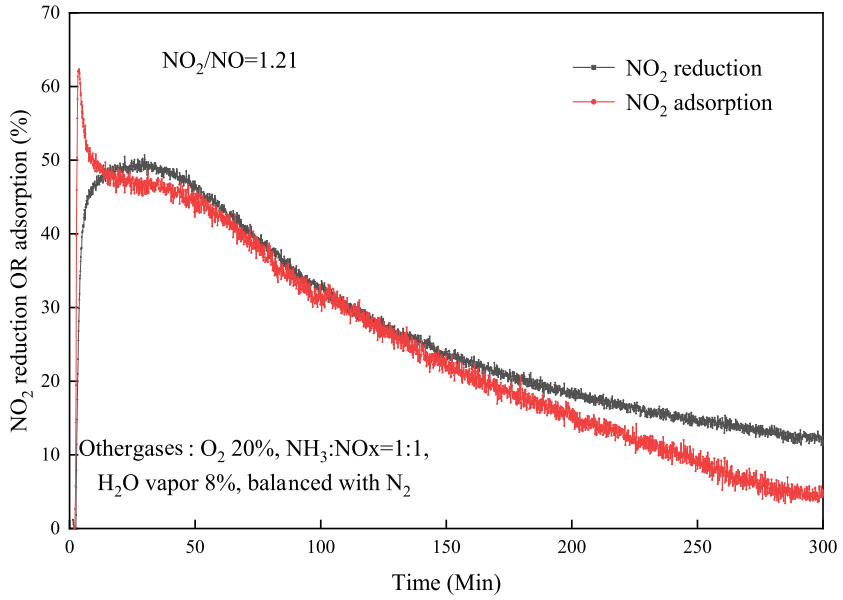


**Figure 8.** $NO_2$ adsorption and reduction over ACs.

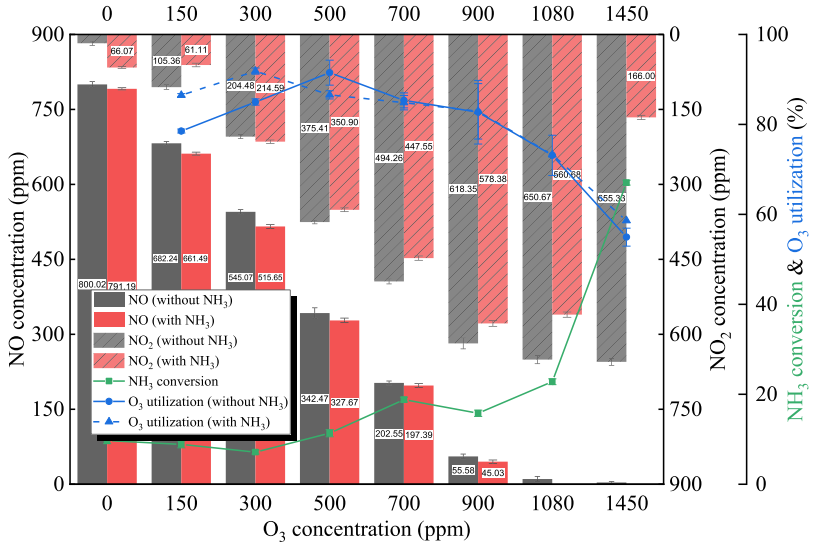


**Figure 9.** Gaseous oxidation of NO by ozone.

$NO_x$ conversion. Ozone oxidation has been considered as a common method for $NO_x$ removal. The effect of $O_3$ on NO oxidation, especially in the presence of $NH_3$, was studied before the mixture went through the fixed-bed reactor containing ACs, and the results are shown in Figure 10.

It can be seen that with the increase of the $O_3$ concentration from 0 to 900 ppm ($O_3$/NO ⇐ 1), the NO concentration sharply dropped, whereas the $NO_2$ concentration increased rapidly whether with or without $NH_3$. With a further increase of the $O_3$ concentration to higher than 900 ppm ($O_3$/NO > 1), the NO concentration dropped to zero for both with and without $NH_3$. The $NO_2$ concentration stabilized at about 650 ppm in the absence of $NH_3$ in the gas mixture. As for gas mixtures with $NH_3$, the $NO_2$ concentration sharply dropped to about 166 ppm at a $O_3$/NO ratio of 1.5. The $NH_3$ conversion rate was 10−20% at $O_3$/NO ⇐ 1, and sharply increased to 67% at $O_3$/NO = 1.5. Furthermore, white crystals were found on the inside wall of the tubes after $NH_3$ addition. The produced crystalline solids were collected and characterized by infrared spectroscopy (IR) using a Fourier-transform infrared spectroscopy (FTIR) spectrometer (Thermo Scientific Nicolet 6700). The sample was mixed with KBr at a weight ratio of 1:200 and milled before being flaked. The IR spectra of the white crystals are shown in Figure 11. According to literature,[41,42] the solid is identified as ammonium nitrate ($NH_4NO_3$). The utilization rate of $O_3$ was around 80% at $O_3$/NO ⇐ 1, which dropped upon further increasing the $O_3$/NO ratio. When $O_3$/NO > 1, $N_2O_5$ was generatedin the gas mixture,[37] which resulted in the decrease of the $O_3$ utilization rate. $N_2O_5$ further reacts with $NH_3$ and produced $NH_4NO_3$,[43] which caused the decrease of the $NO_2$ concentration and the increase of the $NH_3$ conversion rate.

Transient experiments were conducted over ACs in a wet mixture consisting of 900 ppm NO, 500 ppm $O_3$, and the results are in Figure 12. At 100 °C, $NO_x$ conversion after $O_3$ oxidation exhibits a similar trend compared to directly mixing of NO and $NO_2$ at a ratio of 1.21. The produced NO decreased along with $NO_2$ breakthrough. This indicates that


https://doi.org/10.1021/acsomega.1c01722
ACS Omega 2021, 6, 13484−13495

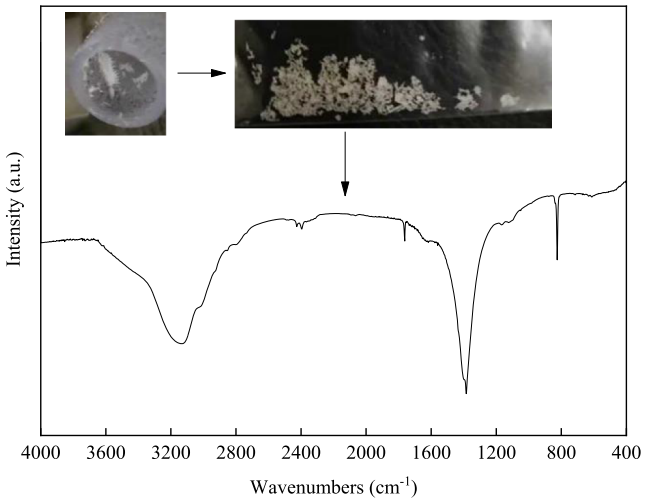


**Figure 10.** IR spectra of the produced crystalline phase in experiment at $O_3$/NO = 1.5.

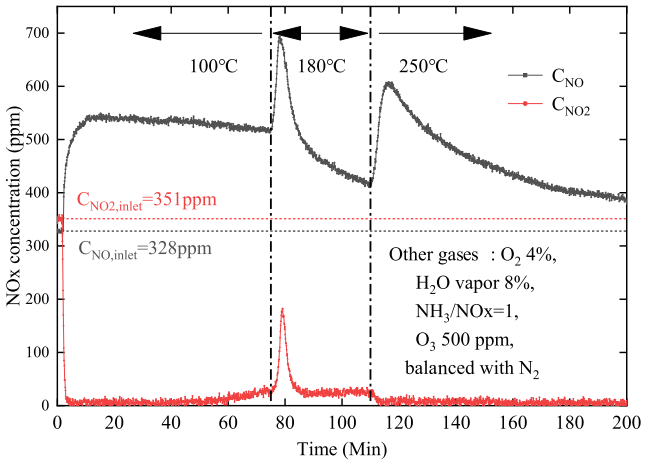


**Figure 11.** $NO_x$ transient conversion over ACs after oxidized with $O_3$ with the effect of temperature.

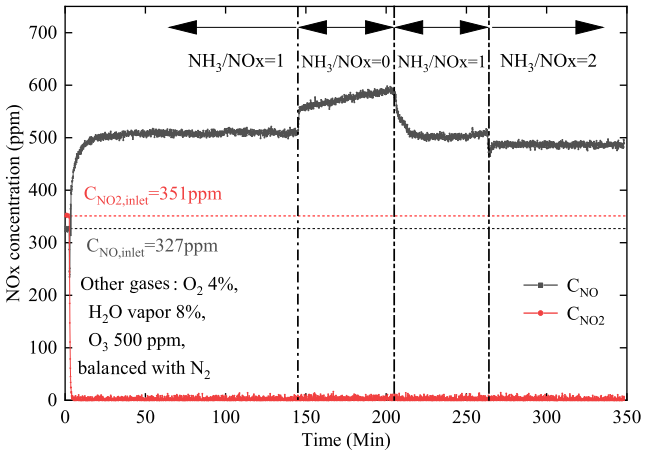


**Figure 12.** $NO_x$ transient conversion over ACs after oxidized with $O_3$ at a low GHSV.

the existence of $O_3$ in the gas mixture exhibits hardly any impact on $NO_x$ conversion over AC when $O_3$/NO ⇐ 1. When the experimental temperature increased to 180 °C, the NO concentration dropped to 413 ppm following a crest. The $NO_2$ concentration stabilized at about 28 ppm after the crest. With the increase of experimental temperature to 250 °C, the NO concentration further decreased to 385 ppm after a crest. The $NO_2$ concentration dropped to nearly zero. The decrease of NO and $NO_2$ concentrations with increasing temperature was attributed to the weakening $NO_2$ adsorption via a disproportionation route and the strengthening fast SCR reaction. The crests of NO and $NO_2$ concentrations at 180 °C and the NO concentration at 250 °C were resulted from the decomposition of deposited $NH_4NO_3$ in the ACs. The results can prove that higher operation temperature can promote total $NO_x$ conversion.

Although increasing the operation temperature is an effective method to enhance $NO_x$ conversion, it is difficult to be achieved in practical applications. Increasing the gas hourly space velocity (GHSV) and the $NH_3/NO_x$ ratio is also believed to be beneficial for $NO_x$ conversion. The $NO_x$ conversion of the gas mixture with different $NH_3/NO_x$ ratios at a low GHSV of only 4500 was studied and the results are shown in Figure 13. Compared with the breakthrough of $NO_2$ in Figures 8 and 12, the $NO_2$ concentration stabilized at near zero for 350 min after putting more ACs in the reactor. This means lower GHSV can contribute to stable $NO_x$ conversion for a longer reaction time. Transient change of $NH_3$ in mixtures effected the NO concentration at the outlet of the reactor. When the $NH_3/NO_x$ ratio was 1 in the gas mixture, the NO concentration stabilized at about 500 ppm, which was approximately 170 ppm higher than the initial NO concentration. Taking $NH_3$ away from mixtures resulted in the increasing of the NO concentration. The NO concentration resumed after $NH_3$ reloaded as $NH_3/NO_x$ = 1. A further increase of the $NH_3/NO_x$ ratio to 2 led to a slight decrease of the NO concentration through the ACs. The NO concentration stabilized at around 490 ppm (10 ppm lower than $NH_3/NO_x$ = 1). The amounts of NO production and $NO_2$ reduction approximately meet the disproportionation route molar ratio. This has demonstrated the domination of the disproportionation route in the process.

## 3. DISCUSSION

**3.1. Reaction Mechanism over ACs.** $NO_x$ conversion mechanisms are summarized in Figure 14. Oxidation of NO by $O_2$ or $O_3$ under both wet and dry conditions as well as in the presence of $NH_3$ was studied before the gas mixture was sent to the fixed bed containing ACs. $O_2$ can oxidize NO with low efficiency, while $O_3$ is more efficient. A slight reduction of NO and $NO_2$ by $NH_3$ was observed. If the $O_3$ concentration was higher than the NO concentration, $NH_4NO_3$ crystals were formed in the gas mixture containing $NH_3$. Moisture plays an important role in determining the conversion routes of $NO_x$ over ACs. Under dry conditions, $NO_x$ conversion was dominated by the disproportionation route if there was no $NH_3$ in the mixture. Obvious fast SCR reaction as well as direct adsorption of $NO_2$ to ACs were found after $NH_3$ was added to gas mixtures. As for wet mixtures, the fast SCR reaction was too weak to be observed under most operating conditions, especially for the gas mixture containing a higher $NO_2$ concentration at 100 °C. The disproportionation reaction dominated under most operation conditions and under wet conditions. Because of the deposition of $-(ONO_2)$ on the ACs, the disproportionation reaction was inhibited, which has resulted in the increase of the outlet $NO_2$ concentration and the decrease of $NO_x$ removal with time. With the breakthrough


https://doi.org/10.1021/acsomega.1c01722
ACS Omega 2021, 6, 13484−13495

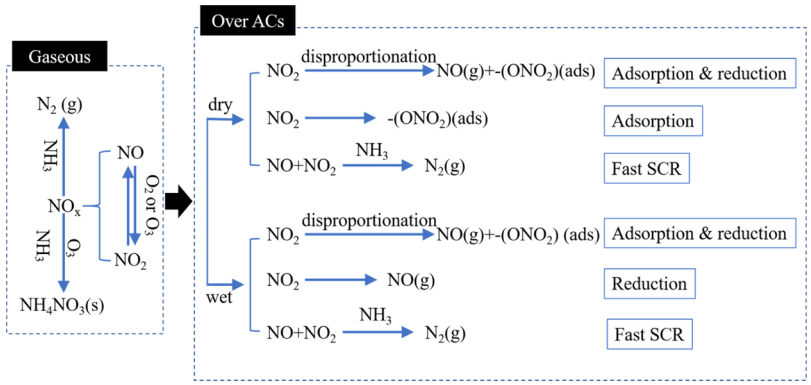


**Figure 13.** $NO_x$ conversion mechanisms in the gaseous phase and over ACs in a highly oxidizing atmosphere.

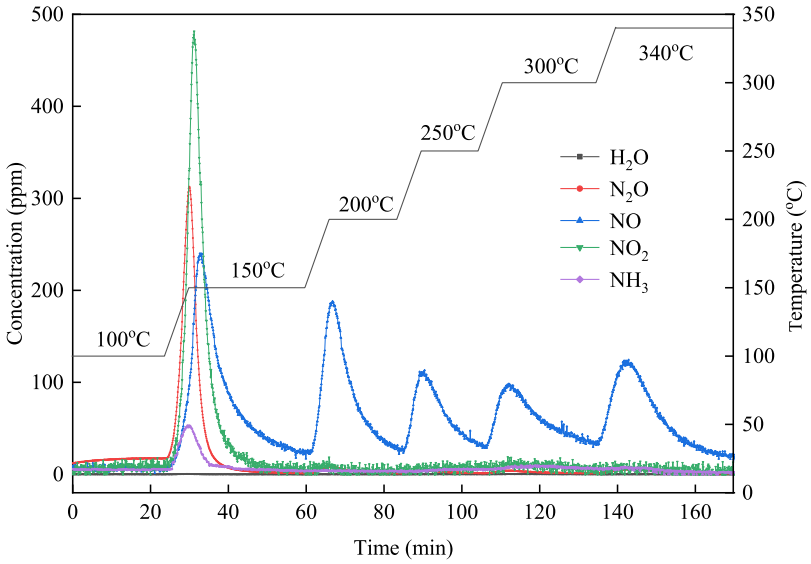


**Figure 14.** Regeneration curves of ACs after the reaction under the conditions of set IV-i.

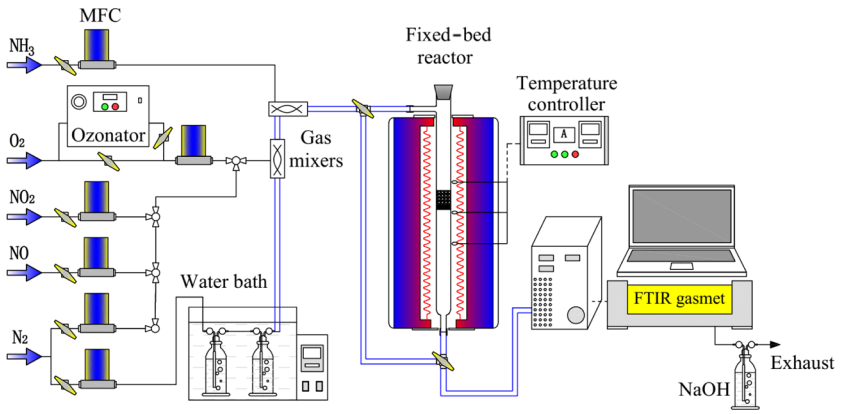


**Figure 15.** Schematic diagram of the fixed-bed experiment system.

of $NO_2$, the $NO_2$ conversion gradually shifted from adsorption via the disproportionation route to direct reduction to NO. Increasing operation temperature can strengthen the fast SCR reaction over ACs, which has become quite important at 250 °C under wet conditions.

**3.2. Method of $NO_x$ Removal with ACs in a Highly Oxidizing Atmosphere.** According to the analysis discussed in section 3, increasing the $NO_2$/NO molar ratio by $O_3$ oxidation can promote $NO_x$ conversion over ACs at 100 °C with moisture in flue gas. The $NO_x$ conversion cannot exceed 50% ($C_{NOx} = C_{NO2}$) due to the dominant disproportionation reaction of $NO_2$ over ACs with one-time oxidation. Increasing operation temperature is an efficient method to break the conversion limit, while energy consumption created difficulties. $NH_3$ is essential in $NO_x$ conversion. Lack of $NH_3$ will resulted in the increase of direct reduction of $NO_2$ to NO over ACs, which is negative for total $NO_x$ conversion. Further study is required to optimize the amount of $NH_3$ added into the flue


https://doi.org/10.1021/acsomega.1c01722
ACS Omega 2021, 6, 13484−13495

gas in order to prevent $NH_3$ escape. The $O_3$/NO ratio should be lower than 1 to prevent the formation of ammonium nitrate in the reactor with $NH_3$.

Considering $-C(ONO_2)$ deposition on ACs via the disproportionation reaction, ACs need to be continuously regenerated to ensure stable $NO_x$ removal efficiency. In the design of reactors, GHSV should be coordinated with AC replacement. AC regeneration can be coupled with $SO_2$-saturated ACs in the regenerator in Figure 1. Products of AC regeneration after $NO_x$ conversion are shown in Figure 15. When temperature increased to 150 °C, NO, $NO_2$, $N_2O$, and $NH_3$ were produced. Upon further increase of temperature, only NO was produced. The released $NO_x$ and $NH_3$ are expected to be further converted into $N_2$ or acid liquor. The produced mixtures by regeneration are characterized by high temperature, low moisture, and low flux, which could be easily converted to $N_2$ with the SCR reaction.

## 4. CONCLUSIONS

Moisture and the oxidizing atmosphere contributed to a significant difference in $NO_x$ conversion both with the gaseous reaction and adsorption/reduction over ACs, especially for $NO_2$ conversion. The disproportionation reaction of $NO_2$ over ACs dominated $NO_x$ conversion under dry conditions with no $NH_3$. Apparent fast SCR was observed under dry conditions with $NH_3$ over the ACs. Under wet conditions, the disproportionation reaction dominated $NO_x$ conversion over ACs both with or without $NH_3$ in the gas mixtures. Increasing the $NO_2$/NO ratio in the gas mixture enhanced the $NO_x$ conversion rate over ACs. $-C(ONO_2)$ deposition on ACs generated by the $NO_2$ disproportionation route resulted in the decrease of the $NO_x$ conversion rate along with the reaction time. $O_3$ oxidation was efficient in increasing the $NO_2$/NO ratio, whereas $NH_3$ is necessary for $NO_x$ conversion under wet conditions. Increasing temperature and decreasing GHSV can promote $NO_x$ conversion over ACs after $O_3$ oxidation. NO oxidation by $O_3$ coupled with $NH_3$ and continuous regeneration of ACs is a potential method for $NO_x$ removal from sintering flue gas.

## 5. MATERIALS AND METHODS

**5.1. Materials and Characterization.** The commercial coal-based AC specialized for desulfurization and denitration was utilized in the study. The ACs received are columnar with a diameter of 9 mm, and were crushed and sieved into particles in the mesh range of 80−150 for this study.

The chemical composition of the sample was determined using an elemental analyzer (Vario EL). The textural properties of the sample were characterized by an automatic surface analyzer (Quantachrome Autosorb 1C) as $N_2$ adsorption/desorption isotherms at 77 K. The specific surface area was calculated by the Brunauer−Emmett−Teller method using the $N_2$ adsorption isotherm. The single-point adsorption method was employed to calculate the total pore volume of the sample. The micropore volume was calculated using the t-plot method. The chemical composition and textural properties of the sample are shown in Table 1.

**5.2. $NO_x$ Adsorption, Reduction, and Desorption Tests.** The $NO_x$ conversion (adsorption and reduction) and desorption tests were carried out using a 500 mm long quartz fixed-bed tube reactor (17 mm i.d.), as shown in Figure 15. All flue gas components except ozone ($O_3$) and water vapor were supplied in cylinders and were mixed in a gas mixer to simulate the flue gas. The flow rate was precisely controlled using mass flow controllers. $O_3$ was made of pure $O_2$ using an ozonator, and water vapor was generated using a heated water bubbler. All the tubes, valves, and joints in contact with $SO_2$ were constructed from either quartz or polytetrafluoroethylene. Moreover, electric-heating tape (Thermolyne) embedded with temperature controllers was used to heat the transport line both upstream and downstream of the fixed-bed reactor to preheat the simulated flue gas and prevent any possible condensation before analysis. The NO, $NO_2$, and $NH_3$ concentrations were monitored and recorded continuously every 5 s using an on-line FTIR spectroscopy gas analyzer (Dx4000, Gasmet Company, Finland). The $O_3$ concentration was analyzed using an ozone monitor (GF-Z-3-50, Shenzhen).

The experimental conditions are summarized in Table 2. In each typical conversion experiment operation, ACs (if required) were put into the glass reactor. Before each experiment, the gas mixtures compositions were measured by FTIR spectroscopy through the bypass of the reactor. When the desired value was reached and stabilized, the gas flow was switched to the glass reactor to start the $NO_x$ conversion and desorption experiments.

$NO_x$ conversion, $NO_2$ adsorption, $NO_2$ reduction, $NH_3$ conversion, and $O_3$ utilization were calculated according to the following equations

$$NO_x \text{ conversion} = \frac{C_{NO_2,inlet} + C_{NO_{inlet}} - C_{NO_2,outlet} - C_{NO_{outlet}}}{C_{NO_2,inlet} + C_{NO_{inlet}}} \times 100\%$$

$$NO_2 \text{ adsorption} = \frac{C_{NO_2,inlet} - C_{NO_2,outlet} - (C_{NO_{outlet}} - C_{NO_{inlet}})}{C_{NO_2,inlet}} \times 100\%$$

$$NO_2 \text{ reduction} = \frac{C_{NO_{outlet}} - C_{NO_{inlet}}}{C_{NO_2,inlet}} \times 100\%$$

$$NH_3 \text{ conversion} = \frac{C_{NH_3,inlet} - C_{NH_3,outlet}}{C_{NH_3,inlet}} \times 100\%$$

$$O_3 \text{ utilization} = \frac{C_{NO,inlet} - C_{NO,outlet}}{C_{O_3,inlet}} \times 100\%$$

where, $C_{NH3,inlet}$ and $C_{NH_3,outlet}$ represent the $NH_3$ concentration (ppm) in the gas mixture at the inlet and outlet of the reactor, respectively, while $C_{NO,inlet}$ and $C_{NO,outlet}$ represent the NO concentration (ppm) in the gas mixture at the inlet and outlet of the reactor, respectively. $C_{O_3,inlet}$ is the $O_3$ concentration (ppm) at the inlet of the reactor.

## AUTHOR INFORMATION

### Corresponding Authors

**Liqiang Zhang** − *National Engineering Laboratory for Reducing Emissions from Coal Combustion, Engineering Research Center of Environmental Thermal Technology of Ministry of Education, Shandong Key Laboratory of Energy Carbon Reduction and Resource Utilization, School of Energy and Power Engineering, Shandong University, Jinan,*



https://doi.org/10.1021/acsomega.1c01722
*ACS Omega* 2021, 6, 13484−13495

*Shandong 250061, China;* orcid.org/0000-0003-1639-2064; Email: zhlq@sdu.edu.cn

**Yong Dong** − *National Engineering Laboratory for Reducing Emissions from Coal Combustion, Engineering Research Center of Environmental Thermal Technology of Ministry of Education, Shandong Key Laboratory of Energy Carbon Reduction and Resource Utilization, School of Energy and Power Engineering, Shandong University, Jinan, Shandong 250061, China;* orcid.org/0000-0002-8530-3857; Email: dongy@sdu.edu.cn

## Authors

**Mengze Zhang** − *National Engineering Laboratory for Reducing Emissions from Coal Combustion, Engineering Research Center of Environmental Thermal Technology of Ministry of Education, Shandong Key Laboratory of Energy Carbon Reduction and Resource Utilization, School of Energy and Power Engineering, Shandong University, Jinan, Shandong 250061, China;* orcid.org/0000-0003-2301-4619

**Xiao Zhu** − *National Engineering Laboratory for Reducing Emissions from Coal Combustion, Engineering Research Center of Environmental Thermal Technology of Ministry of Education, Shandong Key Laboratory of Energy Carbon Reduction and Resource Utilization, School of Energy and Power Engineering, Shandong University, Jinan, Shandong 250061, China*

**Yang Li** − *Xi'an Thermal Power Research Institute Co., Ltd, Xi'an 710054, China*

**Jun Li** − *National Engineering Laboratory for Reducing Emissions from Coal Combustion, Engineering Research Center of Environmental Thermal Technology of Ministry of Education, Shandong Key Laboratory of Energy Carbon Reduction and Resource Utilization, School of Energy and Power Engineering, Shandong University, Jinan, Shandong 250061, China*

**Xiao Xia** − *National Engineering Laboratory for Reducing Emissions from Coal Combustion, Engineering Research Center of Environmental Thermal Technology of Ministry of Education, Shandong Key Laboratory of Energy Carbon Reduction and Resource Utilization, School of Energy and Power Engineering, Shandong University, Jinan, Shandong 250061, China*

**Chunyuan Ma** − *National Engineering Laboratory for Reducing Emissions from Coal Combustion, Engineering Research Center of Environmental Thermal Technology of Ministry of Education, Shandong Key Laboratory of Energy Carbon Reduction and Resource Utilization, School of Energy and Power Engineering, Shandong University, Jinan, Shandong 250061, China*

Complete contact information is available at: https://pubs.acs.org/10.1021/acsomega.1c01722

## Notes

The authors declare no competing financial interest.

## ■ ACKNOWLEDGMENTS

This work was supported by the National Key R&D Program of China (no. 2017YFB0602901).

## ■ REFERENCES

(1) Cui, L.; Li, Y.; Tang, Y.; Shi, Y.; Wang, Q.; Yuan, X.; Kellett, J. Integrated Assessment of the Environmental and Economic Effects of an Ultra-Clean Flue Gas Treatment Process in Coal-Fired Power Plant. *J. Cleaner Prod.* **2018**, *199*, 359−368.

(2) Wang, S.; Yu, X.; Gu, Y.; Yuan, J.; Zhang, Y.; Chen, Y.; Chai, F. Discussion of Emission Limits of Air Pollutants for "Near-Zero Emission" Coal-Fired Power Plants. *Res. Environ. Sci.* **2018**, *31*, 975−984.

(3) Li, Z.; Hu, Y.; Chen, L.; Wang, L.; Fu, D.; Ma, H.; Fan, L.; An, C.; Liu, A. Emission Factors of NOx, SO2, and PM for Bathing, Heating, Power Generation, Coking, and Cement Industries in Shanxi, China: Based on Field Measurement. *Aerosol Air Qual. Res.* **2018**, *18*, 3115−3127.

(4) Cui, L.; Ba, K.; Li, F.; Wang, Q.; Ma, Q.; Yuan, X.; Mu, R.; Hong, J.; Zuo, J. Life Cycle Assessment of Ultra-Low Treatment for Steel Industry Sintering Flue Gas Emissions. *Sci. Total Environ.* **2020**, *725*, 138292.

(5) Bo, X.; Li, Z.; Qu, J.; Cai, B.; Zhou, B.; Sun, L.; Cui, W.; Zhao, X.; Tian, J.; Kan, H. The Spatial-Temporal Pattern of Sintered Flue Gas Emissions in Iron and Steel Enterprises of China. *J. Cleaner Prod.* **2020**, *266*, 121667.

(6) Ministry of Ecology and Environment of the People's Republic of China. Opinions on pushing forward the implementation of ultra-low Emissions in the Steel industry. http://www.mee.gov.cn/xxgk2018/xxgk/xxgk03/201904/t20190429_701463.html. (Accessed 2 November 2020)

(7) Ding, X.; Li, Q.; Wu, D.; Liang, Y.; Xu, X.; Xie, G.; Wei, Y.; Sun, H.; Zhu, C.; Fu, H.; Chen, J. Unexpectedly Increased Particle Emissions from the Steel Industry Determined by Wet/Semidry/Dry Flue Gas Desulfurization Technologies. *Environ. Sci. Technol.* **2019**, *53*, 10361−10370.

(8) Gao, J.; Wang, T.; Shu, Q.; Nawaz, Z.; Wen, Q.; Wang, D.; Wang, J. An Adsorption Kinetic Model for Sulfur Dioxide Adsorption by ZL50 Activated Carbon. *Chin. J. Chem. Eng.* **2010**, *18*, 223−230.

(9) Rosas, J. M.; Ruiz-Rosas, R.; Rodríguez-Mirasol, J.; Cordero, T. Kinetic Study of SO2 Removal over Lignin-Based Activated Carbon. *Chem. Eng. J.* **2017**, *307*, 707−721.

(10) Li, Z.; Liu, Y.; Wang, H.; Tsai, C.-J.; Yang, X.; Xing, Y.; Zhang, C.; Xiao, P.; Webley, P. A. A numerical modelling study of SO2 adsorption on activated carbons with new rate equations. *Chem. Eng. J.* **2018**, *353*, 858−866.

(11) Sun, F.; Gao, J.; Liu, X.; Tang, X.; Wu, S. A Systematic Investigation of SO2 Removal Dynamics by Coal-Based Activated Cokes: The Synergic Enhancement Effect of Hierarchical Pore Configuration and Gas Components. *Appl. Surf. Sci.* **2015**, *357*, 1895−1901.

(12) Li, J.; Zhang, L.; Wang, T.; Chang, J.; Song, Z.; Ma, C. Study on sulfur migration in activated carbon adsorption-desorption cycle: Effect of alkali/alkaline earth metals. *J. Environ. Sci.* **2021**, *99*, 119−129.

(13) Kong, Y.; Cha, C. Y. NOx Adsorption on Char in Presence of Oxygen and Moisture. *Carbon* **1996**, *34*, 1027−1033.

(14) Kaneko, K.; Fukuzaki, N.; Kakei, K.; Suzuki, T.; Ozeki, S. Enhancement of nitric oxide dimerization by micropore fields of activated carbon fibers. *Langmuir* **1989**, *5*, 960−965.

(15) Gao, X.; Liu, S.; Zhang, Y.; Luo, Z.; Ni, M.; Cen, K.; Liu, S.; Gao, X.; Zhang, Y.; Cen, K.; Ni, M. Adsorption and Reduction of NO2 over Activated Carbon at Low Temperature. *Fuel Process. Technol.* **2011**, *92*, 139−146.

(16) Jeguirim, M.; Belhachemi, M.; Limousy, L.; Bennici, S. Adsorption/reduction of nitrogen dioxide on activated carbons: Textural properties versus surface chemistry - A review. *Chem. Eng. J.* **2018**, *347*, 493−504.

(17) Shirahama, N.; Moon, S. H.; Choi, K.-H.; Enjoji, T.; Kawano, S.; Korai, Y.; Tanoura, M.; Mochida, I. Mechanistic Study on Adsorption and Reduction of NO2 over Activated Carbon Fibers. *Carbon* **2002**, *40*, 2605−2611.

(18) Mochida, I.; Kisamori, S.; Hironaka, M.; Kawano, S.; Matsumura, Y.; Yoshikawa, M. Oxidation of NO into NO2 over Active Carbon Fibers. *Energy Fuels* **1994**, *8*, 1341−1344.

(19) Mochida, I.; Kawabuchi, Y.; Kawano, S.; Matsumura, Y.; Yoshikawa, M. High Catalytic Activity of Pitch-Based Activated Carbon Fibres of Moderate Surface Area for Oxidation of NO to NO2 at Room Temperature. *Fuel* **1997**, *76*, 543−548.
(20) Aarna, I.; Suuberg, E. M. A Review of the Kinetics of the Nitric Oxide-Carbon Reaction. *Fuel* **1997**, *76*, 475−491.
(21) Zhu, Z.; Liu, Z.; Liu, S.; Niu, H. A Novel Carbon-Supported Vanadium Oxide Catalyst for NO Reduction with NH3 at Low Temperatures. *Appl. Catal., B* **1999**, *23*, L229−L233.
(22) Szymański, G. S.; Grzybek, T.; Papp, H. Influence of Nitrogen Surface Functionalities on the Catalytic Activity of Activated Carbon in Low Temperature SCR of NOx with NH3. *Catal. Today* **2004**, *90*, 51−59.
(23) Guo, Q.; Jing, W.; Hou, Y.; Huang, Z.; Ma, G.; Han, X.; Sun, D. On the Nature of Oxygen Groups for NH3-SCR of NO over Carbon at Low Temperatures. *Chem. Eng. J.* **2015**, *270*, 41−49.
(24) Damma, D.; Ettireddy, P.; Reddy, B.; Smirniotis, P. A Review of Low Temperature NH3-SCR for Removal of NOx. *Catalysts* **2019**, *9*, 349.
(25) Huang, Z.; Zhu, Z.; Liu, Z. Combined Effect of H2O and SO2 on V2O5/AC Catalysts for NO Reduction with Ammonia at Lower Temperatures. *Appl. Catal., B* **2002**, *39*, 361−368.
(26) Gao, X.; Liu, S.; Zhang, Y.; Du, X.; Luo, Z.; Cen, K. Low Temperature Selective Catalytic Reduction of NO and NO2 with NH3 over Activated Carbon-Supported Vanadium Oxide Catalyst. *Catal. Today* **2011**, *175*, 164−170.
(27) Cai, S.; Hu, H.; Li, H.; Shi, L.; Zhang, D. Design of multi-shell Fe2O3@MnOx@CNTs for the selective catalytic reduction of NO with NH3: improvement of catalytic activity and SO2tolerance. *Nanoscale* **2016**, *8*, 3588−3598.
(28) Ma, Z.; Yang, H.; Li, Q.; Zheng, J.; Zhang, X. Catalytic reduction of NO by NH3 over Fe-Cu-OX/CNTs-TiO2 composites at low temperature. *Appl. Catal., A* **2012**, *427−428*, 43−48.
(29) Tang, X.; Hao, J.; Yi, H.; Li, J. Low-Temperature SCR of NO with NH3 over AC/C Supported Manganese-Based Monolithic Catalysts. *Catal. Today* **2007**, *126*, 406−411.
(30) Wang, P.; Yao, L.; Pu, Y.; Yang, L.; Jiang, X.; Jiang, W. Low-temperature selective catalytic reduction of NOx with NH3 over an activated carbon-carbon nanotube composite material prepared by in situ method. *RSC Adv.* **2019**, *9*, 36658−36663.
(31) Shen, B.; Chen, J.; Yue, S.; Li, G. A Comparative Study of Modified Cotton Biochar and Activated Carbon Based Catalysts in Low Temperature SCR. *Fuel* **2015**, *156*, 47−53.
(32) Cao, L.; Chen, L.; Wu, X.; Ran, R.; Xu, T.; Chen, Z.; Weng, D. TRA and DRIFTS Studies of the Fast SCR Reaction over CeO2/TiO2 Catalyst at Low Temperatures. *Appl. Catal., A* **2018**, *557*, 46−54.
(33) Kato, A.; Matsuda, S.; Kamo, T.; Nakajima, F.; Kuroda, H.; Narita, T. Reaction between nitrogen oxide (NOx) and ammonia on iron oxide-titanium oxide catalyst. *J. Phys. Chem.* **1981**, *85*, 4099−4102.
(34) Ellison, W. Recent Developments in the USA in the Application of FGD-Based Technology for Simultaneous SO2, NOx and Mercury Removal. *Radiation Treatment of Gaseous and Liquid Effluents for Contaminant Removal*; IAEA, 2005; p 77.
(35) Skalska, K.; Miller, J. S.; Ledakowicz, S. Intensification of NOx absorption process by means of ozone injection into exhaust gas stream. *Chem. Eng. Process.* **2012**, *61*, 69−74.
(36) Zhang, J.; Zhang, R.; Chen, X.; Tong, M.; Kang, W.; Guo, S.; Zhou, Y.; Lu, J. Simultaneous Removal of NO and SO2 from Flue Gas by Ozone Oxidation and NaOH Absorption. *Ind. Eng. Chem. Res.* **2014**, *53*, 6450−6456.
(37) Zou, Y.; Liu, X.; Zhu, T.; Tian, M.; Cai, M.; Zhao, Z.; Wu, H. Simultaneous Removal of NOx and SO2 by MgO Combined with O3 Oxidation: The Influencing Factors and O3 Consumption Distributions. *ACS Omega* **2019**, *4*, 21091−21099.
(38) Erme, K.; Jõgi, I. Metal Oxides as Catalysts and Adsorbents in Ozone Oxidation of NOx. *Environ. Sci. Technol.* **2019**, *53*, 5266−5271.
(39) Dastgheib, S. A.; Salih, H.; Ilangovan, T.; Mock, J. NO Oxidation by Activated Carbon Catalysts: Impact of Carbon Characteristics, Pressure, and the Presence of Water. *ACS Omega* **2020**, *5*, 21172−21180.
(40) Jeguirim, M.; Tschamber, V.; Brilhac, J. F.; Ehrburger, P. Interaction Mechanism of NO2 with Carbon Black: Effect of Surface Oxygen Complexes. *J. Anal. Appl. Pyrolysis* **2004**, *72*, 171−181.
(41) Kearley, G. J.; Kettle, S. F. A.; Oxton, I. A. The i.r. Spectra of NH4NO3. *Spectrochim. Acta, Part A* **1980**, *36*, 507−509.
(42) Théorêt, A.; Sandorfy, C. INFRARED SPECTRA AND CRYSTALLINE PHASE TRANSITIONS OF AMMONIUM NITRATE. *Can. J. Chem.* **1964**, *42*, 57−62.
(43) Frenck, C.; Weisweiler, W. Modeling the Reactions Between Ammonia and Dinitrogen Pentoxide to Synthesize Ammonium Dinitramide (ADN). *Chem. Eng. Technol.* **2002**, *25*, 123.


https://doi.org/10.1021/acsomega.1c01722
*ACS Omega* 2021, 6, 13484−13495